



Integration of hyperspectral and LiDAR data for mapping small water bodies

Jiří Prošek^a, Kateřina Gdulová^a, Vojtěch Barták^a, Jiří Vojar^b, Milič Solský^a, Duccio Rocchini^{a,c}, Vítězslav Moudrý^{a,d,*}

^a Department of Applied Geoinformatics and Spatial Planning, Faculty of Environmental Sciences, Czech University of Life Sciences Prague, Kamýcká 129, Praha – Suchbát, 165 00, Czech Republic

^b Department of Ecology, Faculty of Environmental Sciences, Czech University of Life Sciences Prague, Kamýcká 129, Praha – Suchbát, 165 00, Czech Republic

^c Alma Mater Studiorum University of Bologna, Department of Biological, Geological and Environmental Sciences, via Irnerio 42, 40126, Bologna, Italy

^d Institute for Environmental Studies, Faculty of Science, Charles University, Benátská 2, 12801 Prague 2, Czech Republic

ARTICLE INFO

Keywords:

Classification

Fusion

Hyperspectral

LiDAR

Mining

Spoil heap

Water

ABSTRACT

Inland water bodies are globally threatened by environmental degradation and climate change. On the other hand, new water bodies can be designed during landscape restoration (e.g. after coal mining). Effective management of new water resources requires continuous monitoring; in situ surveys are, however, extremely time-demanding. Remote sensing has been widely used for identifying water bodies. However, the use of optical imagery is constrained by accuracy problems related to the difficulty in distinguishing water features from other surfaces with low albedo, such as tree shadows. This is especially true when mapping water bodies of different sizes. To address these problems, we evaluated the potential of integrating hyperspectral data with LiDAR (hereinafter “integrative approach”). The study area consisted of several spoil heaps containing heterogeneous water bodies with a high variability of shape and size. We utilized object-based classification (Support Vector Machine) based on: (i) hyperspectral data; (ii) LiDAR variables; (iii) integration of both datasets. Besides, we classified hyperspectral data using pixel-based approaches (K-mean, spectral angle mapper). Individual approaches (hyperspectral data, LiDAR data and integrative approach) resulted in 2–22.4 % underestimation of the water surface area (i.e. omission error) and 0.4–1.5 % overestimation (i.e., commission error). The integrative approach yielded an improved discrimination of open water surface compared to other approaches (omission error of 2 % and commission error of 0.4 %). We also evaluated the success of detecting individual ponds; the integrative approach was the only one capable of detecting the water bodies with both omission and commission errors below 10 %. Finally, the assessment of misclassification reasons showed a successful elimination of shadows in the integrative approach. Our findings demonstrate that the integration of hyperspectral and LiDAR data can greatly improve the identification of small water bodies and can be applied in practice to support mapping of restoration process.

1. Introduction

Water, besides being an essential natural resource, also represents an important environment supporting biodiversity. Inland water bodies are however globally threatened by agricultural irrigation, ongoing urbanization, environmental degradation and climate change (Vörösmarty et al., 2010), and the spatial and temporal changes of surface water bodies are therefore drawing more and more attention (Pekel et al., 2016). Precise extraction and repeated monitoring of open surface water bodies are needed for better management of water resources as well as for preserving these threatened ecosystems and

preventing biodiversity loss (Harrison et al., 2018).

Mining is one of the human activities with strong environmental impacts (Hendrychová and Kabrna, 2016; Svobodová et al., 2012). In particular, surface mining and associated extensive disturbances significantly influence large areas and negatively affect the freshwater biota; this situation usually persists even after the reclamation of the mining site (Giam et al., 2018; Osenberg, 2018). On the other hand, it has been repeatedly shown that reclaimed areas can have a high conservation value (Schulz and Wiegand, 2000; Vanhée and Devigne, 2018; Vymazal and Sklenicka, 2012). Spoil heaps (i.e. the place where the material discarded during mining is dumped) have been shown to

* Corresponding author at: Department of Applied Geoinformatics and Spatial Planning, Faculty of Environmental Sciences, Czech University of Life Sciences Prague, Kamýcká 129, Praha – Suchbát, 165 00, Czech Republic.

E-mail address: moudry@fzp.czu.cz (V. Moudrý).

<https://doi.org/10.1016/j.jag.2020.102181>

Received 3 November 2019; Received in revised form 2 June 2020; Accepted 12 June 2020

0303-2434/ © 2020 The Authors. Published by Elsevier B.V. This is an open access article under the CC BY license (<http://creativecommons.org/licenses/by/4.0/>).

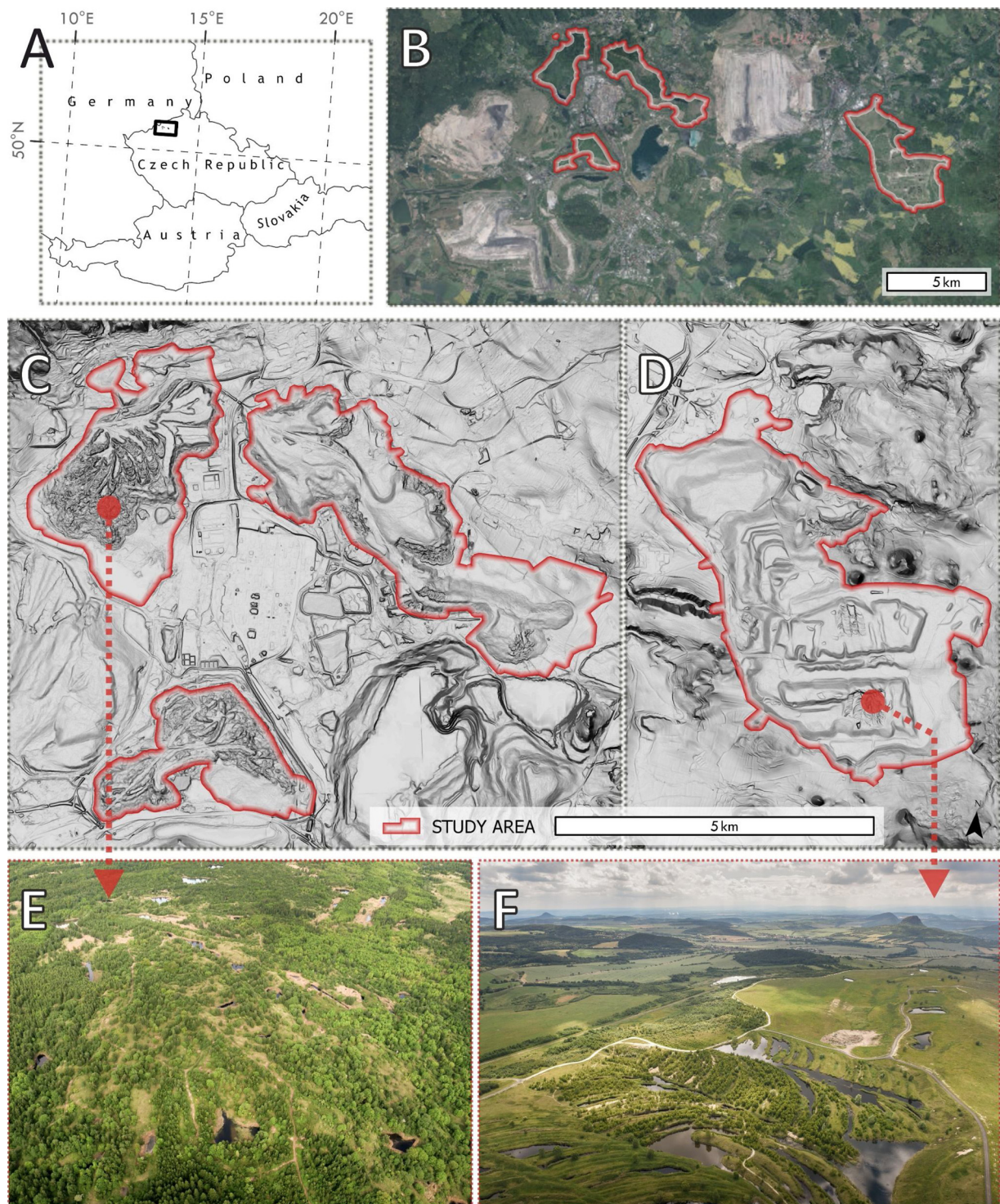


Fig. 1. Study area – (A) The location of the study area within central Europe. (B) The four spoil heaps under study are delineated in red. (C;D) Representation of the topographical and landscape scale context as a combination of slope and hillshade. (E;F) Aerial images of representative water bodies. Images were taken in the time range between 2011 and 2016. (E) Hornojiretinska spoil heap was largely left to spontaneous succession and it is literally dotted with small surface water bodies. (F) Radovesicka spoil heap was mostly technically reclaimed, but note the area at the bottom of the image that was left to spontaneous succession with many surface water bodies.

become important refuges for biodiversity (Harabiš et al., 2013; Vojar et al., 2016). This is particularly true about spoil heaps left to spontaneous succession – such spoil heaps represent habitats that have been disappearing throughout Europe for decades (Doležalová et al., 2012). Leaving the spoil heaps to spontaneous succession is an alternative approach to technical reclamation (Bradshaw, 1997; Prach and Hobbs,

2008). Technical reclamation involves terrain levelling and results in uniform terrain. In contrast, terrain morphology of areas left to spontaneous succession remains rugged as a result of heaping that forms a typical undulated terrain (see Fig. 1). In such a terrain, there are many small depressions filled with water and the density of small water bodies is considerably higher on spoil heaps left to spontaneous

succession than on technically reclaimed sites (Doležalová et al., 2012). These small water bodies are especially valuable for endangered aquatic species such as anurans (Vojar et al., 2016) and dragonflies (Harabiš et al., 2013).

Labour intensive and extremely time demanding in situ surveys are often needed to localize these small water bodies. Such a survey was undertaken for example by Doležalová et al. (2012) who identified more than 900 open surface water bodies important for conservation of water-related taxa on spoil heaps. Although field surveys provide information valuable for preserving important habitats and for understanding of various ecological and environmental processes (e.g. Prach and Walker, 2011), they are often unsuitable for repeated monitoring due to its labour intensiveness. Although remote sensing has been widely used for identification of surface water and for monitoring of surface water changes (see review by Huang et al., 2018), this cost-effective alternative for field surveys is only rarely adopted in restoration projects (Cordell et al., 2017).

Several processing techniques have been adopted for surface water identification (Chen et al., 2004). For example, various spectral water indices are frequently used to extract water bodies due to the ease of use and low computational cost. The Normalized Difference Water Index (NDWI) was developed to distinguish open water bodies from vegetation using green and NIR bands of Landsat satellite images (McFeeters, 1996); several modifications and improvements of that index have been subsequently introduced (Feyisa et al., 2014; Xu, 2006). Another approach is to extract water features using various classification techniques, of which the Support Vector Machine approach is the most popular (Pôssa and Maillard, 2018; Rokni et al., 2015). However, other classification algorithms in combination with various data sources (spectral, LiDAR or radar dataset) have also been used (e.g. neural networks, K-nearest neighbour and random forests) to distinguish water bodies individually (Kaplan and Avdan, 2017; Mahdianpari et al., 2017; Paul et al., 2018) or in the context of several land cover classes (Antonarakis et al., 2008; Brennan and Webster, 2006; Dronova et al., 2015; Luo et al., 2016).

Images from satellite sensors of varying spatial, temporal, and spectral resolution have been extensively used to detect, extract, or assess the quality of surface water. This includes identification of water bodies using satellite sensors such as Landsat Thematic Mapper or MODIS (Carroll et al., 2009; Di Vittorio and Georgakakos, 2018; Lu et al., 2011). Such data are particularly suitable for studies at a relatively coarse resolution (Moudrý et al., 2017; Moudrý and Šimová, 2013). For regional or local scale studies that require detailed information about small water bodies (Šíkola et al., 2019; Šimová et al., 2019), satellite or airborne data with high spatial resolution emerged as an important data source and were utilized for applications such as wetland mapping (Harken and Sugumaran, 2014; McCarthy et al., 2018; Zhang and Xie, 2012), water quality assessment (Giardino et al., 2007; Olmanson et al., 2013; Saylam et al., 2017) and water body identification (Xie et al., 2016, 2014).

However, the use of optical imagery is constrained by accuracy problems. In particular, these are related to the difficulty in distinguishing water features from other surfaces with low albedo, such as shadows of clouds and terrain (Verpoorter et al., 2012). In the case of high-resolution imagery, shadows of high objects (e.g. trees) may also pose a problem (Liu et al., 2017; Mostafa and Abdelhafiz, 2017). The presence of such surfaces may cause misclassification due to the similarity in reflectance patterns. Various approaches have been proposed to overcome this problem (Mostafa and Abdelhafiz, 2017; Verpoorter et al., 2012). Moreover, studies on the causes of problems with water surface identification (especially misclassification for shadows) based only on spectral information (Bochow et al., 2012; Jakovljević et al., 2018; Lu et al., 2011; Shao et al., 2011; Xie et al., 2014; Yang et al., 2018) aimed to identify and map significantly larger water bodies (from hundreds or thousands of square meters, respectively) than ponds present in the post-mining sites. However, correct identification of such

small water ponds typical for post-mining sites is crucial for further environmental research (Doležalová et al., 2012; Šíkola et al., 2019; Vojar et al., 2016).

The above-mentioned problems can be eliminated by combining optical imagery with other remote sensing data such as LiDAR, which provides information complementary to optical images (and vice versa). Combining optical imagery data with additional characteristics such as vegetation height, drainage network or terrain slope is a popular approach (Donchyts et al., 2016; Lu et al., 2011; Mueller et al., 2016). These characteristics can be easily derived from LiDAR and it is increasingly common to have both LiDAR and hyperspectral data available for the same area (Asner et al., 2015, 2007; Hanuš et al., 2016). For example, Maxwell et al. (2014) used the height of objects on the ground and intensity of the returns derived from airborne LiDAR as an additional source to RapidEye satellite imagery for pixel based classification of land cover (including water) at mining sites and mine reclamation areas. Irwin et al. (2017) used optical imagery, synthetic aperture radar and airborne LiDAR independently to develop three separate surface water classifications, which were subsequently combined to create an optimal water surface dataset. More recently, Degerickx et al. (2019) used the height of objects on the ground (low, medium, and high category) derived from airborne LiDAR as an additional data source for sub-pixel classification (spectral unmixing) of urban land cover, but they did not consider water as a separate land cover class. Wu et al. (2019) used multi-temporal aerial imagery to map shallow depressional wetlands of size between 100 m² to 30,000 m² and combined it with surface depressions derived from LiDAR DTM to refine the classification extent.

However, the use of LiDAR in above mentioned studies was often limited and its potential was not fully utilized. For example, LiDAR-derived variables were usually limited to one or combination of two (e.g. objects' height and intensity of the returns; Degerickx et al., 2019; Maxwell et al., 2014), or the use of LiDAR data was limited to simple refinement of optical imagery classification results (e.g. Wu et al., 2019). In this study, we build on the results of above-mentioned studies. We use several LiDAR-derived variables that proved to be valuable for land cover classification and integrate them with hyperspectral data into a single classification approach (hereinafter "integrative approach"). The main objective of this study is to extract open surface water bodies on spoil heaps from very high-resolution airborne data (resolution < 2 m). A crucial step in such a process is the elimination of problems caused by shadows of trees and terrain (i.e. false positives). To achieve this goal, we adopted object-based approach, which is recommended for processing and classification of very high-resolution data (Alonzo et al., 2014; Blaschke, 2010; Liu et al., 2015). Besides, it is quite common that LiDAR and hyperspectral data show a certain level of spatial misalignment (e.g. Parmehr et al., 2014), and object-based classifications are less prone to such misalignment (Blaschke, 2010). To illustrate the advantages of our integrative approach, we compared its results with object-based classification based solely on hyperspectral or LiDAR data, and with the classification of hyperspectral data by two traditional pixel-based approaches. We quantitatively evaluated the accuracy of all above-mentioned classification methods in terms of: (i) overall accuracy per area with stratified random points sampling; (ii) accuracy validated per feature classified as water bodies; and (iii) the sources of misclassification.

2. Materials

2.1. Study area

The present study was conducted on four spoil heaps originating from brown coal mining located in the North Bohemian brown coal basin, the largest mining area in the Czech Republic and one of the largest in all of Europe. The total study area is 37.97 km² and the terrain elevation ranges from 200 m to 410 m above sea level (Fig. 1).

Depending on the age of the spoil heap, adopted reclamation techniques and consequently terrain character, the vegetation consists of forest, steppes (low vegetation with scattered shrubs and trees), grassland, and aquatic vegetation (e.g. Doležalová et al., 2012; Frouz et al., 2018). Spoil heaps also differ in their character due to the application of different reclamation approaches. Some have been technically reclaimed, which led to a formation of a uniform terrain, while others (or their parts) have not and their terrain morphology remained rugged as a result of heaping, forming a typical undulated terrain (Frouz et al., 2018). The number of small water bodies in the study area is especially high in areas without technical terrain reclamation, their sizes ranging from several square meters to thousands of square meters (see Fig. 1). Some water bodies were also artificially created; those are, however, generally larger than those of “natural” origin. The study area therefore contains heterogeneous water bodies with a high variability of shape and size located in environments with contrasting vegetation cover (e.g. grassland, dense shrubs, and forests; see Doležalová et al., 2012 for more details about the character of the water bodies in the study area).

2.2. Airborne data collection and pre-processing

The airborne LiDAR and hyperspectral data were acquired simultaneously on 18th May 2017 using a remote sensing platform FLIS (The Flying Laboratory of Imaging Spectroscopy; Hanuš et al., 2016). FLIS is operated by the Global Change Research Institute (Czech GLOBE) and equipped with an inertial measurement unit (IMU), global navigation satellite system (GNSS) receiver, two hyperspectral sensors (Visible Near Infrared, VNIR, CASI-1500 and Short Wave Infrared, SWIR, SASI-600), and LiDAR sensor (Riegl LMS Q-780) which are all mounted on an aircraft Cessna 208B Grand Caravan (see Table 1 and Table 2 for sensor parameters and data characteristics). Flights for data collection were conducted at an approximate altitude of 1030 m above ground with an average velocity of 110 knots/h (ground speed). The data acquisition took three hours (from 14:30 to 17:30 CEST) and consisted of 41 flight lines. Data were provided in the European terrestrial reference system ETRS-89 and Universal transverse Mercator projection (UTM33 N).

2.2.1. Hyperspectral data

The hyperspectral imagery consisted of 48 bands covering the visible near-infrared range from 380 to 1050 nm (CASI-1500) and 100 bands covering the near-infrared and short-wave infrared range from 950 to 2450 nm (SASI-600) with a bandwidth of 15 nm (Table 1). Pre-processing of the hyperspectral images (i.e., radiometric correction, georeferencing and atmospheric corrections) were all carried out by the provider (Czech GLOBE). Radiometric corrections were performed in the RadCorr software by converting spectral radiances to physical radiance units based on calibration parameters from the CzechGlobe spectroscopic laboratory (Hanus et al., 2016). Resulting images were geometrically corrected and orthorectified based on the aircraft-mounted GNSS/IMU systems and a digital terrain model (namely digital terrain model with 5 m per pixel resolution, provided by the State Administration of Land Surveying and Cadastre). Subsequently, VNIR

Table 1
Hyperspectral sensors and dataset characteristics.

Sensor parameters	Sensor	
	VNIR (CASI-1500)	SWIR (SASI-600)
Spectral resolution [nm]	380 – 1050	950 – 2450
Bandwidth [nm]	15	15
Max. spectral resolution [nm]	3.2	15
Count of band	48	100
Spatial resolution [m/pixel]	0.5	1.25
Angle of view [°]	40	40

Table 2
LiDAR sensor and dataset characteristic.

Sensor Parameters	LiDAR sensor (Riegl LMS Q-780)
Wavelength [nm]	1064
Laser pulse frequency [kHz]	400
Beam divergence [mrad]	0.25
Point density [point/m ²]	7 – 8
Angle of view [°]	60

and SWIR data were merged and resampled to the chosen coordinate system (VNIR data were resampled to SWIR spatial resolution of 1.25 m using the Pixel aggregate method) and corrected for atmospheric conditions using a radiative transfer model MODTRAN in ATCOR-4 software (Richter and Schläpfer, 2016).

2.2.2. LiDAR data

Airborne LiDAR data were acquired using a Riegl LMS Q-780 laser scanner (Table 2). The scanner has a rotating polygon mirror and scans in parallel lines. The scan field of view is 60° and the wavelength is 1064 nm. The LiDAR data were provided in LAZ format with an average point density of 8 points per square meter. We further processed the LiDAR point cloud using LAStools (LAStools, 2019; <http://lastools.org>). LASnoise and LASground tools of the LAStools software were used to identify ground points. We tested several settings for LASground and visually assessed the resulting digital terrain models using hill-shaded terrain and the success of the identification of ground points in the most troublesome areas. The best results were acquired using predefined settings for natural environments (Moudrý et al., 2020, 2019).

Based on the visual inspection and variables used in prior studies (Antonarakis et al., 2008; Lu et al., 2011), we considered the following five variables as suitable for water bodies identification: (i) Point density – number of points per spatial unit; (ii) Intensity – the average light intensity of LiDAR returns; (iii) The ratio of the number of first returns and of all returns; (iv) Elevation of the normalised digital surface model based on the triangular network of points identified as non-ground points; (v) Slope of the digital surface model – based on the triangular network of all first-class returns. All LiDAR variables were derived for identical spatial units and sampled to the same raster grid – cells were aligned with the same spatial resolution of 1.25 m in the UTM 33 N coordinate system. For subsequent classification steps, we created a composite dataset consisting of a full hyperspectral cube (with all 148 bands) and five LiDAR-derived variables (Fig. 2).

3. Methods

3.1. Overview of methodology

To classify open surface water, we adopted the Support Vector Machine (SVM) object-based classification approach. The SVM is a supervised machine learning classification method successfully used for classification of integrated LiDAR and hyperspectral data (Dalponte et al., 2012; Luo et al., 2016; Okiemute and Ruth, 2017). Here, we use SVM in its simplest form as a binary classifier (for more information on this method, see review by Mountrakis et al., 2011 and references therein). We performed object-based classifications using hyperspectral data and LiDAR variables both separately and in combination. In addition, we also used two different pixel-based classification methods based on hyperspectral data; namely, the K-mean classification (a representative of unsupervised classification methods) and the spectral angle mapper (a recommended and optimal method for hyperspectral datasets) were utilised. We also tested the classification based only on NIR and SWIR bands (by simple thresholding) as a part of preliminary testing. However, the results were poor (we faced problems misclassification of water and shadows) and therefore not presented in this study. The failure of simple thresholding was the initial motivation for

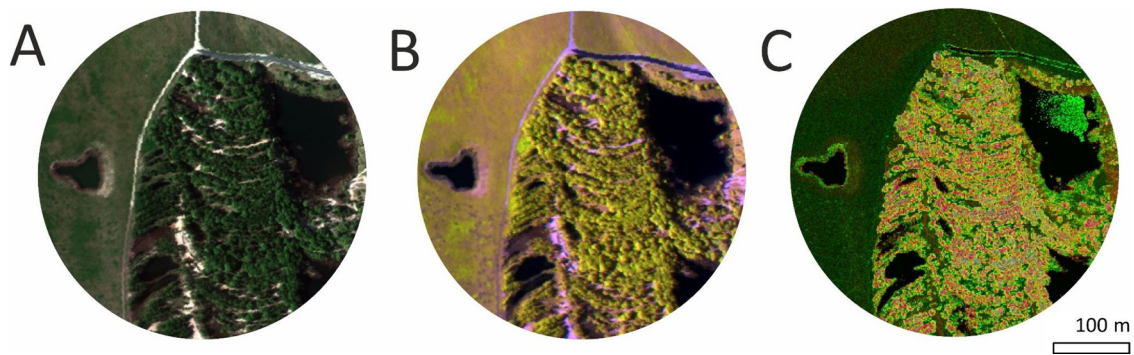


Fig. 2. (A) Aerial photo – true colour composite with RGB bands (i.e., the visible part of the spectrum), (B) false colours composite with Red, NIR, SWIR band (i.e., representation of the infrared part of the spectrum) and (C) LiDAR variables composite where the red band represents nDSM, the green band represents the light intensity of LiDAR returns, and blue represent points density.

the use of more complex classification approaches (e.g. Object-based classification and data integration).

The accuracy of all classifications was quantitatively assessed in terms of: (i) validation per area with stratified random points sampling (i.e. how accurate the individual methods are in the identification of water surface in general); (ii) accuracy validated per feature classified as water bodies (i.e. how successful the individual methods are in detecting the particular ponds or lakes); (iii) sources of misclassification (e.g. land cover, shadow). The major data processing steps and adopted methods are presented in Fig. 3. Data pre-processing and classification were performed in ENVI SW, post-processing and all spatial operations in ArcGIS 10.6 SW (ESRI, Redlands, CA, USA).

3.2. Object-based classification approaches

We used object-based classification approaches based on the Support Vector Machine (SVM) algorithm (specific ENVI software implementation as a representative of object-based classification). First, we performed segmentation by the “Feature Extraction tool” based on similar spectral, textural and shape characteristics, and on LiDAR variables. We iteratively tested combinations of “scale level” and “merge level” input parameters on five samples (100×100 m). After a visual inspection of tests on those preliminary samples, we used the scale level value of 25 and merge level value of 75, or scale level value of 30 and merge level value of 80, depending on the study site.

Second, we used the supervised classification method based on the SVM algorithm independently for (i) full range hyperspectral data; (ii) LiDAR variables; and (iii) combination/composite of hyperspectral data and LiDAR variables. We manually selected 20 representative training samples for each category. The following characteristics per object were used for SVM classification: Basic variables (Mean, Standard Deviation, Min and Max pixel value), Texture variables (Range, Mean, Variance,

Entropy), and Spatial variables (Area, Length, Compactness, Convexity, Roundness, Elongation, Numbers of holes, Hole Area/Solid Area).

3.3. Pixel-based classification approaches

3.3.1. Unsupervised classification approach

K-mean clustering is a typical representative of nonparametric, unsupervised classification approach (Tou and Gonzalez, 1974). We used pixel-based, K-Mean image classification implemented in the ENVI software. The following input parameters were used: number of classes, change threshold, the maximum number of iterations. Using an inappropriate number of classes represents a common problem of this approach (typically a combination of water surface and shadows in one class; Movia et al., 2016). Therefore, we iteratively tested the numbers of classes (a range from 5 to 30) on five samples (100×100 m) while keeping other parameters unchanged (change threshold: 1%, maximum number of iterations: 50). After each iteration, we performed a visual inspection using high-resolution ortho-images (0.5 m per pixel) as a reference. Based on the results of this preliminary test, 12 classes were used in the final classification.

3.3.2. Spectral angle classification approach

Spectral angle mapper (SAM) classification approach determines the spectral similarity between two spectral curves by calculating the angle between the spectral bands (Kruse et al., 1993). Selection of input parameters includes the selection of (1) a suitable calibration dataset (spectral library) and (2) a threshold maximum angle deviation. We assembled a spectral library based on over 200 samples of water bodies in our study area. We iteratively tested and visually inspected the maximum angle deviation in steps of 0.05 units (ranging from 0.05 to 1.0) on five samples (100×100 m) and used the maximum angle deviation of 0.2 for the final experiment.

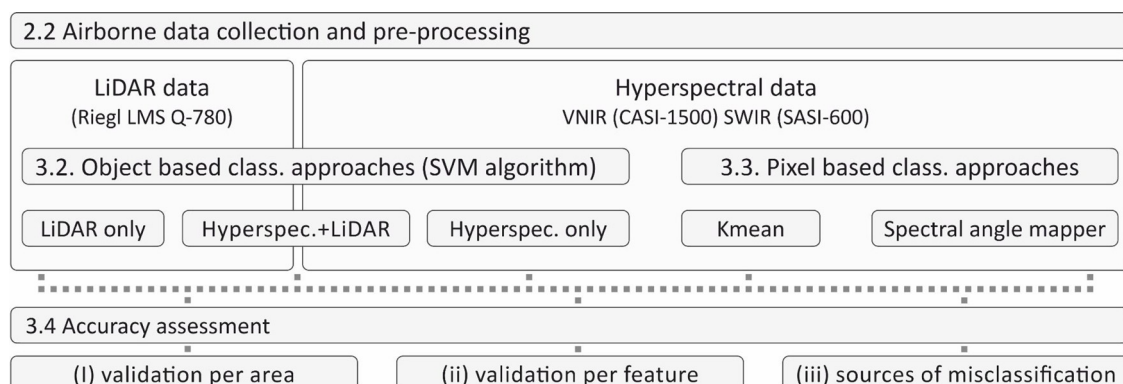


Fig. 3. Study workflow - overview of the methodology, classification approaches and accuracy assessment.

3.4. Accuracy assessment

We quantitatively assessed the accuracy of classification methods in the following way: (i) We used a stratified random sampling design according to the good practices for accuracy assessment (Olofsson et al., 2014) with randomly generated 500 points (hereafter validation per area). 50 % of validation points were generated in non-water and 50 % in water areas.

(ii) We compared the classification approaches based on the accuracy validated “per feature”, i.e. per objects identified as water bodies. We randomly generated 500 points located within features classified as water bodies. Conditions for points sampling were set as follows: no more than a single point was located in each water feature; water features consisting of less than 4 pixels were omitted. 147 of those points were subsequently manually identified (see below) as non-water and 353 as water surface samples.

(iii) We assessed the cause of misclassification (e.g. the presence of spectrally similar land cover categories, such as shadows or categories with similar LiDAR characteristics such as roads or holes in vegetation structure). Those “misclassification points” were generated for each of the classification approaches separately, until we had 100 points where classification failed for each approach. Subsequently, the reasons of misclassifications were analysed (the distribution of misclassification reasons was not significantly changing once the number of points exceeded 100).

For validation per area and validation per feature, we calculated omission and commission error (calculation of accuracy metrics is given in Appendix A1). We calculated the omission error as the fraction of values belonging to the water category but misclassified as non-water (i.e. measure of false negatives that is complement to producer's accuracy) and the commission error as the fraction of values classified as water but not belonging to that class (i.e. measure of false positives that is complement to user's accuracy). All points used for the above validations were assessed over relatively high-resolution ortho-images (0.5 m per pixel) and manually assigned to appropriate categories. To eliminate the possibility of false water identification, this assignment was done by a researcher with expert knowledge of the site and presence or absence of questionable water bodies were verified by a field survey.

4. Results

4.1. Overall accuracy

The methods of identification of water bodies differed in the overall accuracy, especially in the identification of particular water bodies and sources of misclassification. Typical examples of classification results are presented in Fig. 4. The classification accuracy of open surface water bodies based on the validation per area depends on the classification method (Fig. 5 and Table A2), with the omission error ranging from 2 % to 22.4 % and a generally low the commission error – lower than 1.5 % (which is however caused predominantly by the fact that the total area of water bodies is smaller than the total remaining area). The most accurate classification was achieved by the integrative approach (SVM hyperspec. + LiDAR) with omission and commission errors of 2% and 0.4 %, respectively. The object-based classification using only hyperspectral data (SVM hyperspec. only) had a relatively high omission (7.6 %) as well as commission (1.3 %) errors. The object classification based on LiDAR variables (SVM LiDAR only) had a slightly lower omission error than the K-mean classification (4% compared to 5.2 % for K-mean), and the commission error was in both approaches lower than 1%. SAM classification approach also had a low commission error (0.5 %), but the omission error was the highest of all approaches (22.4 %).

4.2. Per feature accuracy

Validation per feature showed that the integrative approach is more successful in identifying particular water bodies than other methods (Fig. 5 and Table A2). It was the only approach that at the same time correctly identified more than 90 % of water bodies (omission error 5.3 %) as well as more than 90 % of non-water surfaces (commission error 9.6 %). In contrast, object classification based on hyperspectral characteristics only has the highest omission error of 19.4 % as well as a very high commission error of 30.4 %. The remaining methods achieved mutually comparable results with the exception of the SAM classification that yielded the highest commission error (Fig. 5 and Table A2).

4.3. The cause of misclassification

The assessment of misclassification reasons showed that all classifications based solely on hyperspectral data were negatively affected by the presence of shadows and to a certain extent by the presence of artificial surfaces and terrestrial or littoral vegetation (Fig. 6 and Table A3). For all three classification methods based solely on hyperspectral data, more than 50 % of misclassifications were caused by shadows (for a typical example of misclassification, see Fig. 7). The method most affected by shadows was the unsupervised K-mean classification where 73 out of 100 misclassification points were shadows misclassified as water areas. In SAM and SVM, 56 and 51 out of 100 misclassified points were shadows. In contrast, the information provided by LiDAR variables captured major differences between the water surface and shadows (see Fig. 8). In effect, only 4 out of 100 misclassified points were affected by shadows in the classification based on LiDAR variables; its results were rather affected by other categories (in particular vegetation and artificial surface – roads). Classification with integrated LiDAR + hyperspectral data also showed minimum errors caused by the presence of shadows (Fig. 6 and Table A3). The predominant source of misclassification in this method was littoral vegetation, responsible for 87 % of misclassifications.

5. Discussion

In this study, we examined the possibility to integrate airborne LiDAR and hyperspectral data to classify open surface water bodies and in particular to mitigate the negative effect of shadows caused by their spectral signature similar to water. We used a range of structural variables derived from LiDAR and spectral, textural and spatial variables derived from full range hyperspectral data (with 148 bands). We tested both LiDAR variables and hyperspectral data separately and in combination.

Our results show that integration of hyperspectral and LiDAR data improves the water surface classification accuracy. The results are comparable to those reported by Luo et al. (2016) who also integrated airborne LiDAR and hyperspectral data to classify land cover (including water surface) with an omission error of 3.95 % and a zero commission error. Their study area, however, included few water bodies and only 22 validation points were used to evaluate that category. In contrast, Okiemute and Ruth (2017) classified water surface in the context of seven land cover categories, integrating LiDAR and multispectral/hyperspectral data, and achieved a low omission error of 0% and relatively high commission error ranging from 19.6 % to 4.3 %, depending on the classification method.

However, a standard overall accuracy assessment based on validation per area does not accurately reflect the classification accuracy of small water bodies that were our main interest. A standard overall accuracy assessment is biased due to the presence of large water bodies and because the total area of water bodies is smaller than the total remaining area. Therefore, to better characterize the success of identification of water bodies, we also included the “validation per feature”

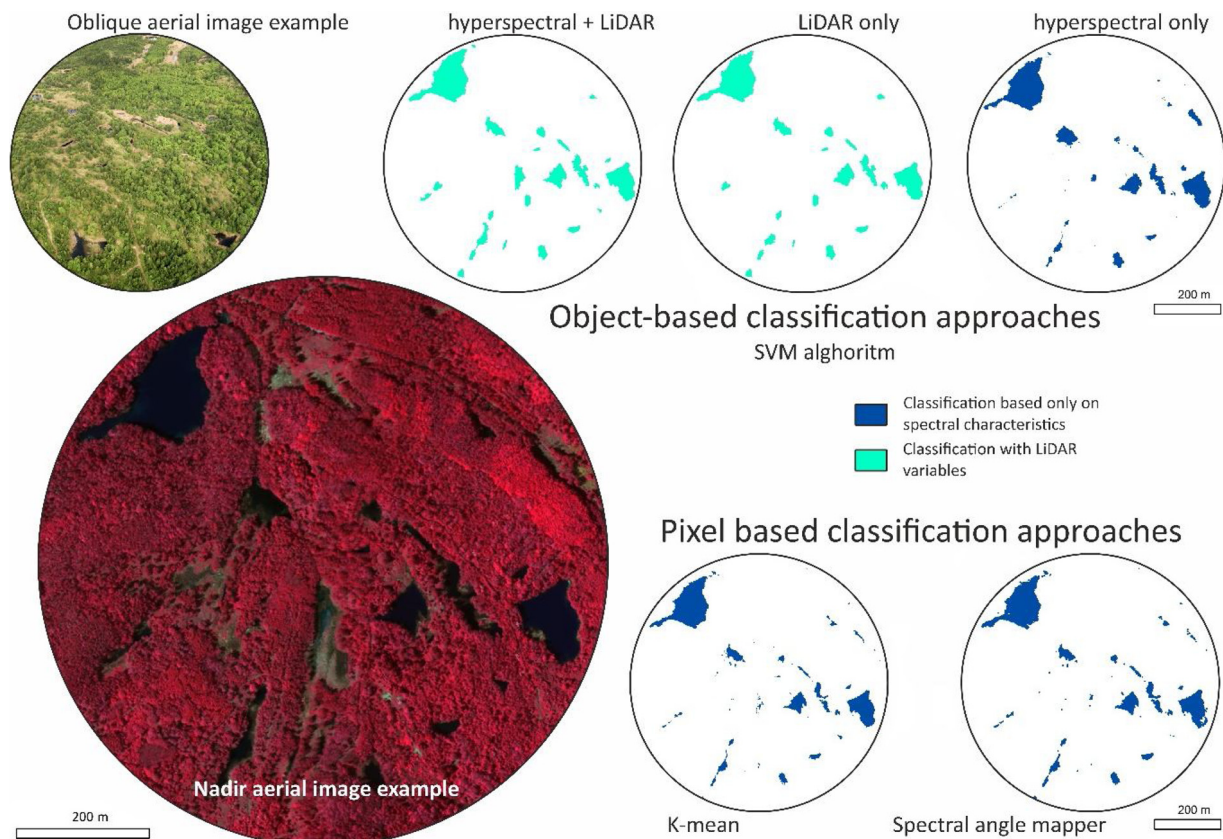


Fig. 4. Example of results of classification approaches and algorithms with classified water bodies at the Hornojiretinska spoil heap (an example of a spoil heap left to a spontaneous succession with hundreds of small water bodies). Note the substantial number of false positives when using only hyperspectral data, which were removed by including LiDAR variables into classification. In addition, classification results demonstrate the differences between the object based approaches (producing compact water bodies) and the pixel based approaches (identifying the classified water bodies as scattered smaller objects).

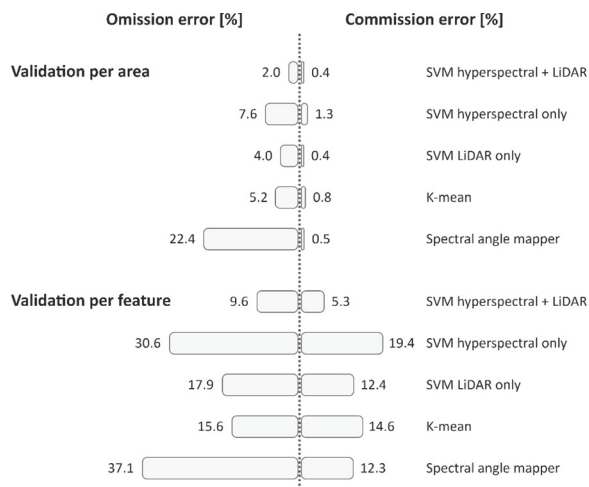


Fig. 5. Results of the accuracy assessment for each classification approach 1) Validation per area based on 250 water and 250 non-water randomly generated validation points; 2) Validation per feature based on 353 water and 147 non-water samples.

(success of detecting individual ponds). Both (validation per area and validation per feature) show similar relative differences between classifications results and demonstrate the benefit of the integrative approach for classification accuracy (for comparison of results of individual validation approaches, see Fig. 5 and Table A2). Moreover, validation per feature shows that the integrative approach is more successful in detecting individual water bodies (including small water

bodies) than remaining classification approaches.

The integrative approach (i.e. the fusion of hyperspectral data and LiDAR variables) improves the classification of water bodies derived from remote sensing data, predominantly by eliminating misclassification problems caused by shadows. Shadows are a common problem of airborne imagery and many studies reported misclassification due to the presence of shadows (Liu et al., 2017; Mostafa and Abdelhafiz, 2017; Verpoorter et al., 2012; Wu et al., 2014). Similar to those, our study also shows that all classification approaches based solely on hyperspectral data are negatively affected by shadows. In contrast, artificial surfaces and terrestrial or littoral vegetation represent a predominant problem for the classification approach based only on LiDAR variables (Fig. 6 and Table A3). It is also noteworthy that our results suggest that the accuracy of the detailed water surface identification based on LiDAR variables alone is comparable to that obtained using hyperspectral data alone (see also Antonarakis et al., 2008).

Although data acquisition during the solar noon is a logical solution for avoiding shadows, it is difficult to accomplish. It is a solution often used with unmanned aerial vehicles (e.g. Cunliffe et al., 2016; Prošek and Šimová, 2019; Weil et al., 2017); however, even if data are acquired during the solar noon, shadows in regions outside the equatorial zone are not fully eliminated. Furthermore, with aircraft used over larger areas, it is impossible to acquire data in a short time and in many parts of the world, weather conditions may pose a problem for a survey. Bad weather conditions also appeared in 2017 in our study area and we had to wait until data acquisition was possible. Wu et al. (2014) suggested an interesting possibility for the elimination of the problem with shaded areas based on a difference between images acquired at different times. This method is, however, suitable only for satellites or unmanned aerial vehicles, not for aircraft data acquisition as double

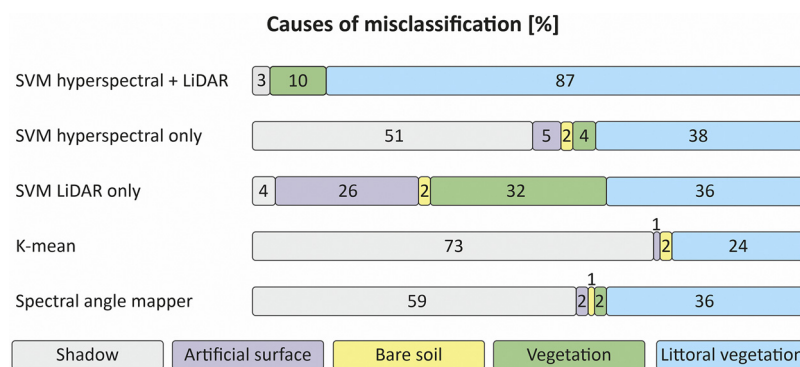


Fig. 6. Causes of misclassification for each classification approach based on 100 validation points.

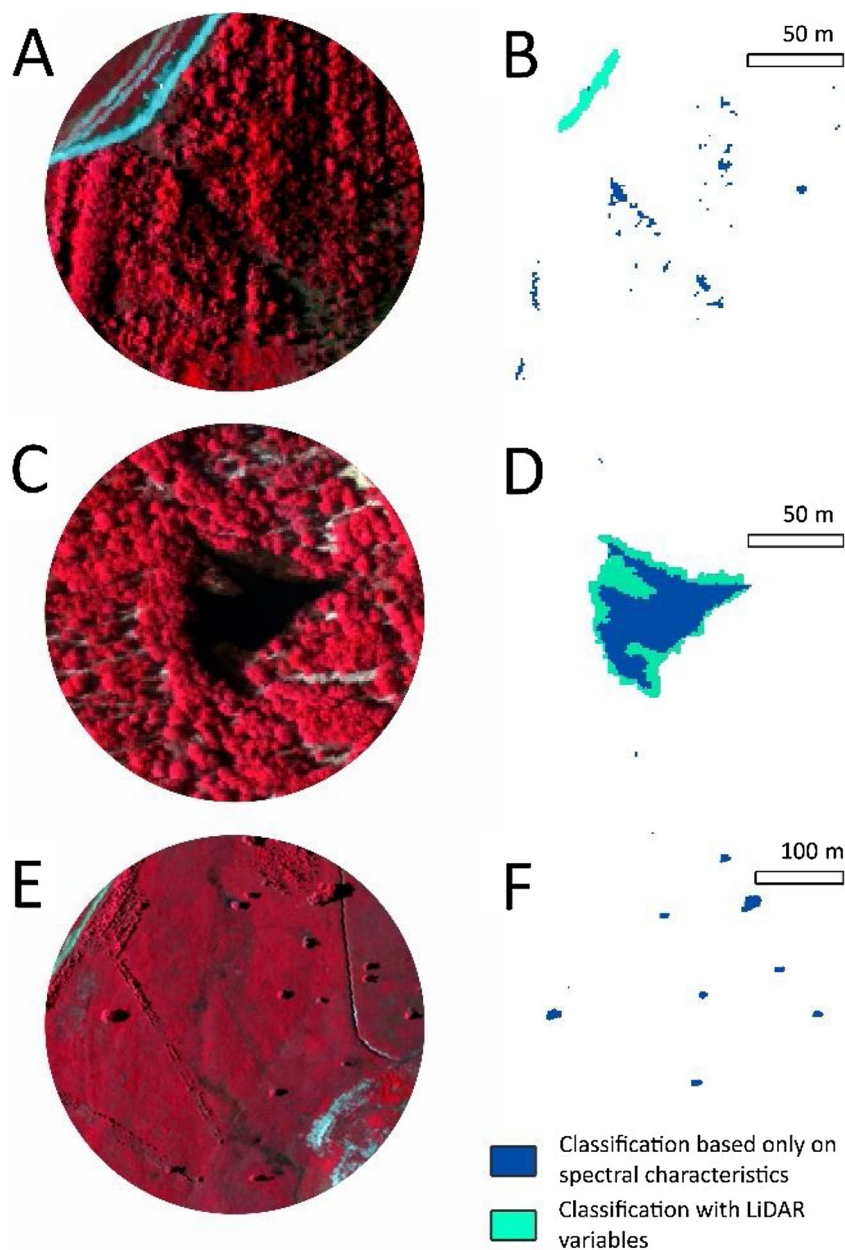


Fig. 7. Examples of typical misclassification reasons. (A;B) Representation of typical misclassification due to shadows in a dense forest (B – dark blue colour) and typical LiDAR misclassification on artificial surfaces (B – light blue colour); (C;D) A typical example of misclassification where object-based classification approach including LiDAR variables classifies the littoral vegetation as a water body (D – light blue colour); (E;F) Example of misclassification where shadows of solitary trees were classified as small water bodies.

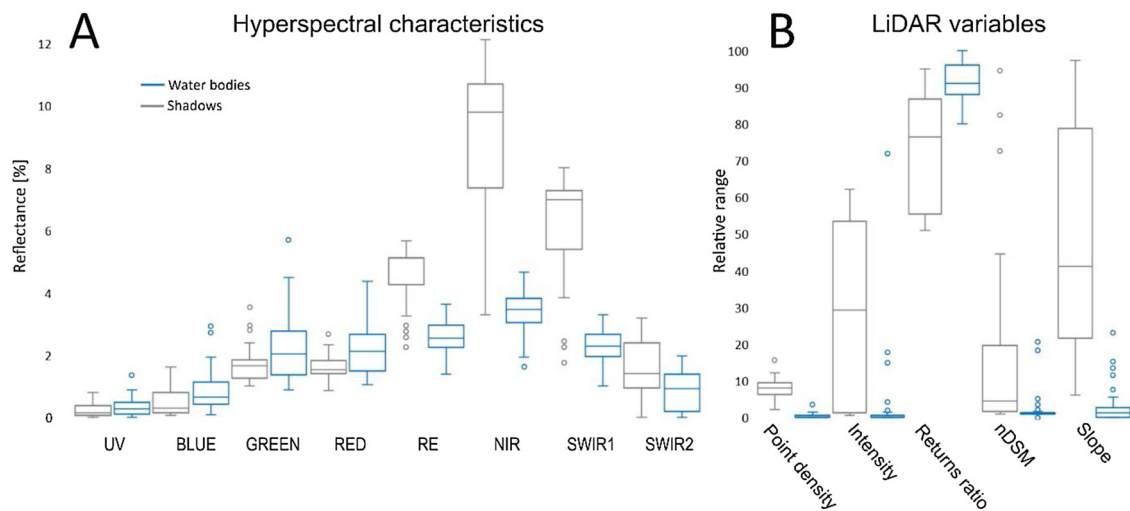


Fig. 8. (A) Distribution of hyperspectral characteristics (represented by relative surface reflectance) demonstrates the similarity in distributions (overlapping variances and similar spectral curves) of most spectral variables between categories of water surface and shadows. (B) LiDAR variables (represented by absolute values of parameters linearly resampled to scale in a range from 0 to 100) show large differences in distributions of LiDAR variables (both in central tendencies and variances) between the water surface and shadows categories. Based on 100 independent samples of both water surface and shadows, together representing more than 1k individual pixels.

recording would incur substantial additional costs.

Littoral vegetation (i.e. non-submerged aquatic vegetation; see Fig. 9 for a typical example) was the predominant source of misclassification in the integrative approach. As the littoral zone is a part of the water body, this misclassification should nevertheless not be considered as an error (Gairola et al., 2013; Husson et al., 2016). We suggest that the combination of LiDAR and hyperspectral data is applicable even where surface water bodies are partly covered by vegetation (e.g. littoral zones), moreover, the combination of LiDAR and hyperspectral data can also improve detection of water bodies even

under the vegetation canopy (e.g. high trees).

We also tested the integration of hyperspectral and LiDAR data with pixel-based approaches; however, the results were poor and therefore not presented in this study. We attribute this failure to misalignment between the two datasets. Hyperspectral and LiDAR data integration in pixel-based classification approaches requires reduction of misalignment of image pixels and LiDAR laser spots issues to a minimum. This is especially problematic when data originate from different platforms. However, even when the data are acquired from the same aircraft, perfect alignment is not guaranteed. To perfectly align the data, several

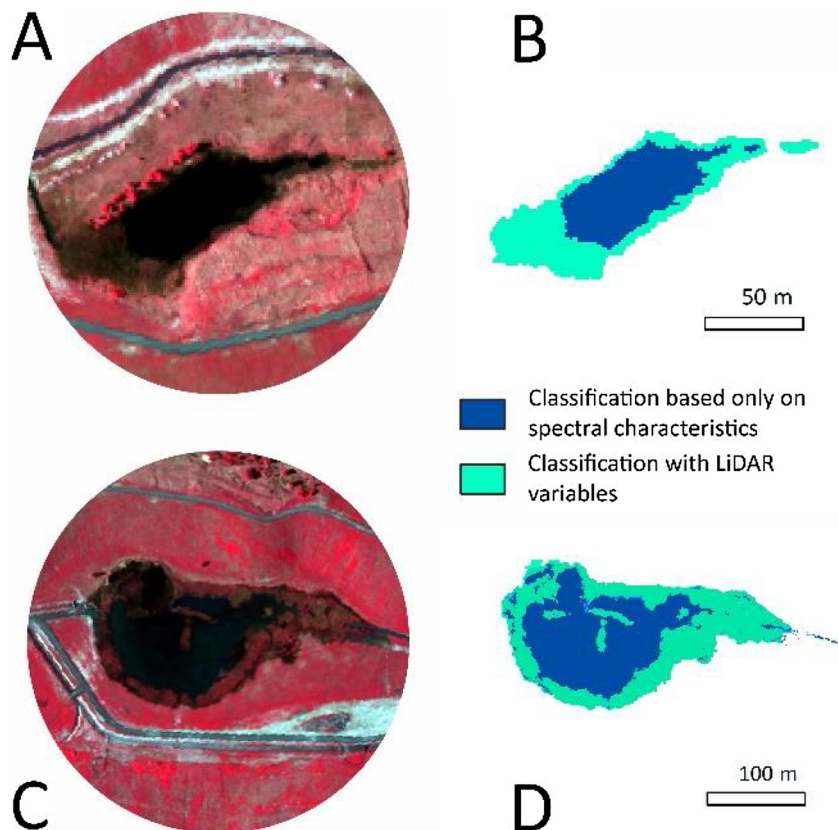


Fig. 9. Example of typical differences between classifications based solely on hyperspectral data (represented by the dark blue colour in C and D) and classification including LiDAR variables (light blue in C and D). Note that water surface with slightly different colour due to the presence of submerged vegetation was not classified as water surface when using only hyperspectral data.

integration steps are required, from placing the instruments on board of the aircraft to a precise time registration of each measurement and final data fusion (Asner et al., 2012). In contrast, object-based classification is considered less prone to problems with noise and edge mixed pixels (Alonzo et al., 2014; Blaschke et al., 2014).

Optical imagery and LiDAR data provide complementary information that can be conveniently integrated to map small water bodies. Although our study area is relatively small (~40 km²), the data integration is limited only by its availability and it has been shown that slight temporal misalignment between acquisition does not cause any major problems for object-based approaches (Irwin et al., 2017). LiDAR data availability is increasing continuously due to national or regional scanning campaigns and the data are often available even free of charge (see Melin et al., 2017 for the list of countries with LiDAR data available). We emphasize that there is a high potential for usage of integrated optical/LiDAR data, such as adopted in this study, in the management of water resources and restoration ecology in general.

6. Conclusion

In this study, we extracted open surface water bodies on spoil heaps at a very high resolution. We used the object-based classification and integrated hyperspectral/LiDAR data. To evaluate the advantages of the integrated data approach, we compared it with classifications using LiDAR and hyperspectral data separately and with two pixel-based approaches with hyperspectral data alone. Our results show that the integrative approach provides better results than the separate use of the datasets and significantly reduces both omission and commission errors. Furthermore, the commission error of the integrative approach was predominantly caused by identifying littoral zones of ponds as water surfaces and in principle should not be considered as an error per se. On the other hand, where hyperspectral data alone were used, shadows were the principal misclassification reason. Most importantly, both the LiDAR-only and integrative approach classifications successfully eliminated problems with shadows that have affected all other approaches. We suggest that the integration of hyperspectral and LiDAR data for open surface water classification can greatly improve the identification of small water bodies and its repeated monitoring, which is crucial for preserving these important habitats not only in our study area but worldwide.

Funding

This work was supported by the Czech Science Foundation under Grant No. 17-17156Y and by the Internal Grant Agency of the Faculty of Environmental Sciences, Czech University of Life Sciences Prague < /GS2 > , under grant No. 20184240.

CRedit authorship contribution statement

Jiří Prošek: Writing - original draft, Writing - review & editing, Conceptualization, Methodology, Validation, Formal analysis, Data curation, Investigation, Visualization. **Kateřina Gdulová:** Writing - original draft, Writing - review & editing, Writing - review & editing, Validation, Investigation. **Vojtěch Barták:** Writing - original draft, Writing - review & editing, Formal analysis. **Jiří Vojar:** Writing - original draft, Writing - review & editing. **Milič Solský:** Writing - original draft, Writing - review & editing. **Duccio Rocchini:** Writing - original draft, Writing - review & editing. **Vítězslav Moudrý:** Writing - original draft, Writing - review & editing, Conceptualization, Investigation, Resources, Supervision, Project administration, Funding acquisition.

Declaration of Competing Interest

The authors declare that they have no known competing financial

interests or personal relationships that could have appeared to influence the work reported in this paper.

Acknowledgements

We are grateful to three anonymous reviewers for their constructive comments that significantly improved the quality of the manuscript. We would also like to thank Markéta Hendrychová for providing aerial photos documenting the spoil heap areas.

Appendix A. Supplementary data

Supplementary material related to this article can be found, in the online version, at doi:<https://doi.org/10.1016/j.jag.2020.102181>.

References

- Alonzo, M., Bookhagen, B., Roberts, D.A., 2014. Urban tree species mapping using hyperspectral and lidar data fusion. *Remote Sens. Environ.* 148, 70–83. <https://doi.org/10.1016/j.rse.2014.03.018>.
- Antonarakis, S., Richards, K.S., Brasington, J., 2008. Object-based land cover classification using airborne LiDAR. *Remote Sens. Environ.* 112, 2988–2998. <https://doi.org/10.1016/j.rse.2008.02.004>.
- Asner, G.P., Asner, G.P., Knapp, D.E., Kennedy-Bowdoin, T., Jones, M.O., Martin, R.E., Boardman, J.W., Field, C.B., 2007. Carnegie Airborne Observatory: in-flight fusion of hyperspectral imaging and waveform light detection and ranging for three-dimensional studies of ecosystems. *J. Appl. Remote Sens.* 1, 013536. <https://doi.org/10.1117/1.2794018>.
- Asner, G.P., Knapp, D.E., Boardman, J., Green, R.O., Kennedy-bowdoin, T., Eastwood, M., Martin, R.E., Anderson, C., Field, C.B., 2012. Carnegie Airborne Observatory-2: increasing science data dimensionality via high-fidelity multi-sensor fusion. *Remote Sens. Environ.* 124, 454–465. <https://doi.org/10.1016/j.rse.2012.06.012>.
- Asner, G.P., Martin, R.E., Anderson, C.B., Knapp, D.E., 2015. Remote Sensing of Environment Quantifying forest canopy traits: imaging spectroscopy versus field survey. *Remote Sens. Environ.* 158, 15–27. <https://doi.org/10.1016/j.rse.2014.11.011>.
- Blaschke, T., 2010. Object based image analysis for remote sensing. *ISPRS J. Photogramm. Remote Sens.* 65, 2–16. <https://doi.org/10.1016/j.isprsjprs.2009.06.004>.
- Blaschke, T., Hay, G.J., Kelly, M., Lang, S., Hofmann, P., Addink, E., Queiroz Feitosa, R., van der Meer, F., van der Werff, H., van Coillie, F., Tiede, D., 2014. Geographic Object-Based Image Analysis - towards a new paradigm. *ISPRS J. Photogramm. Remote Sens.* 87, 180–191. <https://doi.org/10.1016/j.isprsjprs.2013.09.014>.
- Bochow, M., Heim, B., Küster, T., Rogas, C., Bartsch, I., Segl, K., Kaufmann, H., 2012. Automatic detection and delineation of surface water bodies in airborne hyperspectral data. 2012 IEEE International Geoscience and Remote Sensing Symposium. IEEE 5226–5229.
- Bradshaw, A., 1997. Restoration of mined lands—using natural processes. *Ecol. Eng.* 8, 255–269.
- Brennan, R., Webster, T.L., 2006. Object-oriented land cover classification of lidar-derived surfaces. *Can. J. Remote. Sens.* 32, 162–172.
- Carroll, M.L., Townshend, J.R., Dimiceli, C.M., Noojipady, P., Sohlberg, R.A., Townshend, J.R., Dimiceli, C.M., Noojipady, P., Sohlberg, R.A., 2009. A new global raster water mask at 250 m resolution. *Int. J. Digit. Earth* 8947. <https://doi.org/10.1080/17538940902951401>.
- Chen, Q., Zhang, Y., Ekroos, A., Hallikainen, M., 2004. The role of remote sensing technology in the EU water framework directive (WFD). *Environ. Sci. Policy* 7, 267–276. <https://doi.org/10.1016/j.envsci.2004.05.002>.
- Cordell, S., Questad, E.J., Asner, G.P., Kinney, K.M., Thaxton, J.M., Uwolo, A., Brooks, S., Chynoweth, M.W., 2017. Remote sensing for restoration planning : how the big picture can inform stakeholders. *Restor. Ecol.* 25, 147–154. <https://doi.org/10.1111/rec.12448>.
- Cunliffe, A.M., Brazier, R.E., Anderson, K., 2016. Ultra-fine grain landscape-scale quantification of dryland vegetation structure with drone-acquired structure-from-motion photogrammetry. *Remote Sens. Environ.* 183, 129–143. <https://doi.org/10.1016/j.rse.2016.05.019>.
- Dalponte, M., Bruzzone, L., Gianelle, D., 2012. Tree species classification in the Southern Alps based on the fusion of very high geometrical resolution multispectral / hyperspectral images and LiDAR data. *Remote Sens. Environ.* 123, 258–270. <https://doi.org/10.1016/j.rse.2012.03.013>.
- Degerickx, J., Roberts, D.A., Somers, B., 2019. Enhancing the performance of Multiple Endmember Spectral Mixture Analysis (MESMA) for urban land cover mapping using airborne lidar data and band selection. *Remote Sens. Environ.* 221, 260–273. <https://doi.org/10.1016/j.rse.2018.11.026>.
- Di Vittorio, C.A., Georgakakos, A.P., 2018. Land cover classification and wetland inundation mapping using MODIS. *Remote Sens. Environ.* 204, 1–17.
- Doležalová, J., Vojar, J., Smolová, D., Solský, M., Kopecký, O., 2012. Technical reclamation and spontaneous succession produce different water habitats: a case study from Czech post-mining sites. *Ecol. Eng.* 43, 5–12. <https://doi.org/10.1016/j.ecoleng.2011.11.017>.

- Donchyts, G., Schellekens, J., Winsemius, H., Eisemann, E., Van de Giesen, N., 2016. A 30 m resolution surface water mask including estimation of positional and thematic differences using landsat 8, srtm and openstreetmap: a case study in the Murray-Darling Basin, Australia. *Remote Sens. Environ.* 158, 386.
- Dronova, I., Gong, P., Wang, L., Zhong, L., 2015. Mapping dynamic cover types in a large seasonally flooded wetland using extended principal component analysis and object-based classification. *Remote Sens. Environ.* 158, 193–206. <https://doi.org/10.1016/j.rse.2014.10.027>.
- Feyisa, G.L., Meilby, H., Fensholt, R., Proud, S.R., 2014. Automated Water Extraction Index: a new technique for surface water mapping using Landsat imagery. *Remote Sens. Environ.* 140, 23–35. <https://doi.org/10.1016/j.rse.2013.08.029>.
- Frouz, J., Mudrák, O., Reitschmiedová, E., Walmsley, A., Vachová, P., Šimáčková, H., Albrechtová, J., Moradi, J., Kučera, J., 2018. Rough wave-like heaped overburden promotes establishment of woody vegetation while leveling promotes grasses during unassisted post mining site development. *J. Environ. Manage.* 205, 50–58. <https://doi.org/10.1016/j.jenvman.2017.09.065>.
- Gairola, S., Procheş, Ş., Rocchini, D., 2013. High-resolution satellite remote sensing: a new frontier for biodiversity exploration in Indian Himalayan forests. *Int. J. Remote Sens.* 34, 2006–2022. <https://doi.org/10.1080/01431161.2012.730161>.
- Giam, X., Olden, J.D., Simberloff, D., 2018. Impact of coal mining on stream biodiversity in the US and its regulatory implications. *Nat. Sustain.* 1, 176–183. <https://doi.org/10.1038/s41893-018-0048-6>.
- Giardino, C., Brando, V.E., Dekker, A.G., Strömbeck, N., Candiani, G., 2007. Assessment of water quality in Lake Garda (Italy) using Hyperion. *Remote Sens. Environ.* 109, 183–195. <https://doi.org/10.1016/j.rse.2006.12.017>.
- Hanuš, J., Fabián, T.K., Fajmon, L., 2016. Potential of airborne imaging spectroscopy at Czechglobe. *Int. Arch. Photogramm. Remote Sens. Spat. Inf. Sci. XLI*, 15–17. <https://doi.org/10.5194/isprsarchives-XLI-B1-15-2016>.
- Harabiš, F., Tichanek, F., Tropek, R., 2013. Dragonflies of freshwater pools in lignite spoil heaps: restoration management, habitat structure and conservation value. *Ecol. Eng.* 55, 51–61. <https://doi.org/10.1016/j.ecoleng.2013.02.007>.
- Harken, J., Sugumaran, R., 2014. Classification of Iowa wetlands using an airborne hyperspectral image: a comparison of the spectral angle mapper classifier and an object-oriented approach. *Can. J. Remote Sens.* 31, 167–174.
- Harrison, I., Abell, R., Darwall, W., Thieme, M.L., Tickner, D., Timboe, I., 2018. The freshwater biodiversity crisis. *Science (80-)* 362 <https://doi.org/10.1126/science.aav9242>. 1369.1–1369.
- Hendrychová, M., Kabrna, M., 2016. An analysis of 200-year-long changes in a landscape affected by large-scale surface coal mining: history, present and future. *Appl. Geogr.* 74, 151–159. <https://doi.org/10.1016/j.apgeog.2016.07.009>.
- Huang, C., Chen, Y., Zhang, S., Wu, J., 2018. Detecting, extracting, and monitoring surface water from space using optical sensors: a review. *Rev. Geophys.* 56, 333–360.
- Husson, E., Ecke, F., Reese, H., 2016. Comparison of manual mapping and automated object-based image analysis of non-submerged aquatic vegetation from very-high-resolution UAS images. *Remote Sens.* 8, 1–18. <https://doi.org/10.3390/rs8090724>.
- Irwin, K., Beaulne, D., Braun, A., Fotopoulos, G., 2017. Fusion of SAR, optical imagery and airborne LiDAR for surface water detection. *Remote Sens.* 9, 890.
- Jakovljević, G., Govedarica, M., Álvarez-taboada, F., Jakovljević, G., Govedarica, M., Álvarez-taboada, F., 2018. Waterbody mapping: a comparison of remotely sensed and GIS open data sources Waterbody mapping: a comparison of remotely sensed and GIS open data sources. *Remote Sens.* 00, 1–29. <https://doi.org/10.1080/01431161.2018.1538584>.
- Kaplan, G., Avdan, U., 2017. Object-based water body extraction model using Sentinel-2 satellite imagery. *Eur. J. Remote Sens.* 50. <https://doi.org/10.1080/22797254.2017.1297540>.
- Kruse, F.A., Lefkoff, A.B., Boardman, J.B., Heidebrecht, K.B., Shapiro, A.T., Barloon, P.J., Goetz, A.F.H., 1993. The spectral image processing system (SIPS) - interactive visualization and analysis of imaging spectrometer data. *Remote Sens. Environ.* 44, 145–163.
- Liu, J., Li, P., Wang, X., 2015. A new segmentation method for very high resolution imagery using spectral and morphological information. *ISPRS J. Photogramm. Remote Sens.* 101, 145–162. <https://doi.org/10.1016/j.isprsjprs.2014.11.009>.
- Liu, X., Hou, Z., Shi, Z., Bo, Y., Cheng, J., 2017. A shadow identification method using vegetation indices derived from hyperspectral data. *Int. J. Remote Sens.* 38, 5357–5373. <https://doi.org/10.1080/01431161.2017.1338785>.
- Lu, S., Wu, B., Yan, N., Wang, H., 2011. Water body mapping method with HJ-1A/B satellite imagery. *Int. J. Appl. Earth Obs. Geoinf.* 13, 428–434. <https://doi.org/10.1016/j.jag.2010.09.006>.
- Luo, S., Wang, C., Xi, X., Zeng, H., Li, D., Xia, S., Wang, P., 2016. Fusion of airborne discrete-return LiDAR and hyperspectral data for land cover classification. *Remote Sens.* 8, 19. <https://doi.org/10.3390/rs8010003>.
- Mahdianpari, M., Salehi, B., Mohammadimanesh, F., Motagh, M., 2017. Random forest wetland classification using ALOS-2 L-band, RADARSAT-2 C-band, and TerraSAR-X imagery. *ISPRS J. Photogramm. Remote Sens.* 130, 13–31. <https://doi.org/10.1016/j.isprsjprs.2017.05.010>.
- Maxwell, A.E., Warner, T.A., Strager, M.P., Pal, M., 2014. Combining RapidEye satellite imagery and Lidar for mapping of mining and mine reclamation. *Photogramm. Eng. Remote Sens.* 80, 179–189.
- McCarthy, M.J., Radabaugh, K.R., Moyer, R.P., Muller-Karger, F.E., 2018. Enabling efficient, large-scale high-spatial resolution wetland mapping using satellites. *Remote Sens. Environ.* 208, 189–201.
- McFeeters, S.K., 1996. The use of the Normalized Difference Water Index (NDWI) in the delineation of open water features. *Int. J. Remote Sens.* 17, 1425–1432. <https://doi.org/10.1080/01431169608948714>.
- Melin, M., Shapiro, A., Glover-Kapfer, P., 2017. Lidar for Ecology and Conservation. WWF Conservation Technology Series 1 (3), WWF-UK, Woking, United Kingdom.
- Mostafa, Y., Abdelhafiz, A., 2017. Shadow Identification in High Resolution Satellite Images in the Presence of Water Regions. pp. 87–94. <https://doi.org/10.14358/PERS.83.2.87>.
- Moudrý, V., Šímová, P., 2013. Relative importance of climate, topography, and habitats for breeding wetland birds with different latitudinal distributions in the Czech Republic. *Appl. Geogr.* 44. <https://doi.org/10.1016/j.apgeog.2013.08.001>.
- Moudrý, V., Komárek, J., Šímová, P., 2017. Which breeding bird categories should we use in models of species distribution? *Ecol. Indic.* 74, 526–529.
- Moudrý, V., Gdulová, K., Fogl, M., Klápště, P., Urban, R., Komárek, J., Moudrá, L., Štroner, M., Barták, V., Solský, M., 2019. Comparison of leaf-off and leaf-on combined UAV imagery and airborne LiDAR for assessment of a post-mining site terrain and vegetation structure: prospects for monitoring hazards and restoration success. *Appl. Geogr.* 104, 32–41. <https://doi.org/10.1016/j.apgeog.2019.02.002>.
- Moudrý, V., Klápště, P., Fogl, M., Gdulová, K., Barták, V., Urban, R., 2020. Assessment of LiDAR ground filtering algorithms for determining ground surface of non-natural terrain overgrown with forest and steppe vegetation. *Measurement* 150, 107047.
- Mountrakis, G., Im, J., Ogole, C., 2011. ISPRS Journal of Photogrammetry and Remote Sensing Support vector machines in remote sensing: a review. *ISPRS J. Photogramm. Remote Sens.* 66, 247–259. <https://doi.org/10.1016/j.isprsjprs.2010.11.001>.
- Movia, A., Beinat, A., Crosilla, F., 2016. Shadow detection and removal in RGB VHR images for land use unsupervised classification. *ISPRS J. Photogramm. Remote Sens.* 119, 485–495. <https://doi.org/10.1016/j.isprsjprs.2016.05.004>.
- Mueller, N., Lewis, A., Roberts, D., Ring, S., Melrose, R., Sixsmith, J., Lymburner, L., McIntyre, A., Tan, P., Curnow, S., 2016. Water observations from space: mapping surface water from 25 years of Landsat imagery across Australia. *Remote Sens. Environ.* 174, 341–352.
- Okiemute, A., Ruth, A., 2017. Object-based habitat mapping using very high spatial resolution multispectral and hyperspectral imagery with LiDAR data. *Int. J. Appl. Earth Obs. Geoinf.* 59, 79–91. <https://doi.org/10.1016/j.jag.2017.03.007>.
- Olmanon, L.G., Brezonik, P.L., Bauer, M.E., 2013. Airborne hyperspectral remote sensing to assess spatial distribution of water quality characteristics in large rivers: the Mississippi River and its tributaries in Minnesota. *Remote Sens. Environ.* 130, 254–265. <https://doi.org/10.1016/j.rse.2012.11.023>.
- Olofsson, P., Foody, G.M., Herold, M., Stehman, S.V., Woodcock, C.E., Wulder, M.A., 2014. Good practices for estimating area and assessing accuracy of land change. *Remote Sens. Environ.* 148, 42–57. <https://doi.org/10.1016/j.rse.2014.02.015>.
- Osenberg, C.W., 2018. No clean coal for stream animals. *Nat. Sustain.* 1, 160–161. <https://doi.org/10.1038/s41893-018-0049-5>.
- Parmehr, E.G., Fraser, C.S., Zhang, C., Leach, J., 2014. Automatic registration of optical imagery with 3D LiDAR data using statistical similarity. *ISPRS J. Photogramm. Remote Sens.* 88, 28–40. <https://doi.org/10.1016/j.isprsjprs.2013.11.015>.
- Paul, A., Tripathi, D., Dutta, D., 2018. Application and comparison of advanced supervised classifiers in extraction of water bodies from remote sensing images. *Sustain. Water Resour. Manag.* 4, 905–919. <https://doi.org/10.1007/s40899-017-0184-6>.
- Pekel, J.F., Cottam, A., Gorelick, N., Belward, A.S., 2016. High-resolution mapping of global surface water and its long-term changes. *Nature* 540, 418.
- Póssa, É.M., Maillard, P., 2018. Precise delineation of small water bodies from Sentinel-1 data using support vector machine classification precise delineation of small water bodies from Sentinel-1 data using. *Can. J. Remote Sens.* 44, 179–190. <https://doi.org/10.1080/07107038992.2018.1478723>.
- Prach, K., Hobbs, R.J., 2008. Spontaneous succession versus technical reclamation in the restoration of disturbed sites. *Restor. Ecol.* 16, 363–366.
- Prach, K., Walker, L.R., 2011. Four opportunities for studies of ecological succession. *Trends Ecol. Evol.* 26, 119–123. <https://doi.org/10.1016/j.tree.2010.12.007>.
- Prošek, J., Šímová, P., 2019. UAV for mapping shrubland vegetation: does fusion of spectral and vertical information derived from a single sensor increase the classification accuracy? *Int. J. Appl. Earth Obs. Geoinf.* 75, 151–162. <https://doi.org/10.1016/j.jag.2018.10.009>.
- Richter, R., Schläpfer, D., 2016. ATCOR-4 user guide. Ger. Aerosp. Center, Ger 7.0.3, 565–01.
- Rokni, K., Ahmad, A., Solaimani, K., Hazini, S., 2015. A new approach for surface water change detection: integration of pixel level image fusion and image classification techniques. *Int. J. Appl. Earth Obs. Geoinf.* 34, 226–234. <https://doi.org/10.1016/j.jag.2014.08.014>.
- Saylam, K., Brown, R.A., Hupp, J.R., 2017. Assessment of depth and turbidity with airborne Lidar bathymetry and multiband satellite imagery in shallow water bodies of the Alaskan North Slope. *Int. J. Appl. Earth Obs. Geoinf.* 58, 191–200.
- Schulz, F., Wiegand, G., 2000. Development options of natural habitats in a post-mining landscape. *Land Degrad. Dev.* 11, 99–110.
- Shao, Y., Taff, G.N., Walsh, S.J., 2011. Shadow detection and building-height estimation using IKONOS data. *Int. J. Remote Sens.* 32, 6929–6944. <https://doi.org/10.1080/01431161.2010.517226>.
- Šíkola, M., Chajma, P., Anděl, P., Solský, M., Vojar, J., 2019. Finding water: reliability of remote-sensing methods in searching for water bodies within diverse landscapes. *Ecohydrol. Hydrobiol.* 1–10. <https://doi.org/10.1016/j.ecohyd.2019.01.001>.
- Šímová, P., Moudrý, V., Komárek, J., Hrach, K., Fortin, M.-J., 2019. Fine scale waterbody data improve prediction of waterbird occurrence despite coarse scale data. *Ecography (Cop.)* 42, 511–520. <https://doi.org/10.1111/ecog.03724>.
- Svobodova, K., Sklenicka, P., Molnarova, K., Salek, M., 2012. Visual preferences for physical attributes of mining and post-mining landscapes with respect to the socio-demographic characteristics of respondents. *Ecol. Eng.* 43, 34–44. <https://doi.org/10.1016/j.ecoleng.2011.08.007>.
- Tou, J.T., Gonzalez, R.C., 1974. Pattern Recognition Principles. Addison-Wesley Publ. Co.
- Vanhee, B., Devigne, C., 2018. Differences in collembola species assemblages (Arthropoda) between spoil tips and surrounding environments are dependent on vegetation development. *Sci. Rep.* 8, 18067. <https://doi.org/10.1038/s41598-018-01848-6>.

- 36315-1.
- Verpoorter, C., Kutser, T., Tranvik, L., 2012. Oceanography: Methods Automated Mapping of Water Bodies Using Landsat Multispectral Data. pp. 1037–1050. <https://doi.org/10.4319/lom.2012.10.1037>.
- Vojar, J., Doležalová, J., Milič, S., Smolová, D., Kopecký, O., Kadlec, T., Knapp, M., 2016. Spontaneous succession on spoil banks supports amphibian diversity and abundance rich Kopecky. *Ecol. Eng.* 90, 278–284. <https://doi.org/10.1016/j.ecoleng.2016.01.028>.
- Vörösmarty, C.J., McIntyre, P.B., Gessner, M.O., Dudgeon, D., Prusevich, A., Green, P., et al., 2010. Rivers in crisis: global water insecurity for humans and biodiversity. *Nature* 467, 555–561.
- Vymazal, J., Sklenicka, P., 2012. Restoration of areas affected by mining. *Ecol. Eng.* 43, 1–4. <https://doi.org/10.1016/j.ecoleng.2012.02.008>.
- Weil, G., Lensky, I., Resheff, Y., Levin, N., 2017. Optimizing the timing of unmanned aerial vehicle image acquisition for applied mapping of woody vegetation species using feature selection. *Remote Sens.* 9, 1130. <https://doi.org/10.3390/rs9111130>.
- Wu, S.T., Hsieh, Y.T., Chen, C.T., Chen, J.C., 2014. A comparison of 4 shadow compensation techniques for land cover classification of shaded areas from high radiometric resolution aerial images. *Can. J. Remote Sens.* 40, 315–326. <https://doi.org/10.1080/07038992.2014.979488>.
- Wu, Q., Lane, C.R., Li, X., Zhao, K., Zhou, Y., Clinton, N., DeVries, B., Golden, H.E., Lang, M.W., 2019. Integrating LiDAR data and multi-temporal aerial imagery to map wetland inundation dynamics using Google Earth Engine. *Remote Sens. Environ.* 228, 1–13.
- Xie, H., Luo, X., Xu, X., Tong, X., Jin, Y., Pan, H., Zhou, B., 2014. New hyperspectral difference water index for the extraction of urban water bodies by the use of airborne hyperspectral images. *J. Appl. Remote Sens.* 8, 15.
- Xie, C., Huang, X., Zeng, W., Fang, X., 2016. A novel water index for urban high-resolution eight-band WorldView-2 imagery. *Int. J. Digit. Earth* 9, 925–941.
- Xu, H., 2006. Modification of normalised difference water index NDWI to enhance open water features in remotely sensed imagery. *Int. J. Remote Sens.* 27, 9.
- Yang, X., Qin, Q., Grussenmeyer, P., Koehl, M., 2018. Urban surface water body detection with suppressed built-up noise based on water indices from Sentinel-2 MSI imagery. *Remote Sens. Environ.* 219, 259–270. <https://doi.org/10.1016/j.rse.2018.09.016>.
- Zhang, C., Xie, Z., 2012. Combining object-based texture measures with a neural network for vegetation mapping in the Everglades from hyperspectral imagery. *Remote Sens. Environ.* 124, 310–320. <https://doi.org/10.1016/j.rse.2012.05.015>.